

# Observation of the Goos-Hänchen shift in graphene via weak measurements

Shizhen Chen, Chengquan Mi, Liang Cai, Mengxia Liu, Hailu Luo,\* and Shuangchun Wen

Laboratory for spin photonics, School of Physics and Microelectronics Science, Hunan University, Changsha 410082, China

(Dated: September 5, 2016)

We report the observation of the Goos-Hänchen effect in graphene via a weak value amplification scheme. We demonstrate that the amplified Goos-Hänchen shift in weak measurements is sensitive to the variation of graphene layers. Combining the Goos-Hänchen effect with weak measurements may provide important applications in characterizing the parameters of graphene.

Keywords: Polarization, Optics at surfaces, Instrumentation, metrology

The behavior of plane wave in reflection can be simply predicted by geometrical optics. However, for the bounded beam of light, it may undergo extra shifts due to the occurrence of diffractive corrections. Such shifts are known as the Goos-Hänchen (GH) [1] and the Imbert-Fedorov [2, 3] shifts according to the directions parallel and perpendicular to the plane of incidence, respectively. In recent years, the research of the GH shift is still active although it was discovered more than 60 years ago. The corresponding studies reach not only to the investigation of the inherent physics behind this phenomenon [4–8], but also to the behavior of the shift at various reflecting surfaces [9–14], especially the theoretical works of the GH shift in reflection from a graphene-dielectric interface. The system with graphene is very interesting for the observation of beam shifts due to its flexible optical properties. The Fresnel reflection coefficients with the existence of graphene become different [15, 16], and the behavior of the GH shift is changed or tunable [17, 18]. In particular, the GH shift on a substrate coated with graphene can be quantized in an external magnetic field [19]. Even though in a common environment, a giant GH shift in graphene was observed recently [20].

In this paper, we investigate the GH shift in graphene under a total internal reflection (TIR) condition. Like other beam shifts, the GH is generally very small and difficult to be directly observed. Here we amplify it via a weak measurement technique to overcome this difficulty. Interestingly, we find that the shift amplified by a weak value scheme is sensitive to the graphene layers. Weak measurements are an important and convenient approach that has reached fruitful achievements for detecting light beam shifts [21–24]. This novel conception was first proposed in the context of quantum mechanics and then has been extensively studied [25–28]. With the help of weak measurements, the GH shift in TIR [29] or in partial reflection [30] can be observed recently. In our work, the GH shift occurs in the regime of TIR (the reflected intensity is equal to incident intensity), and the success rate of the postselection is still large due to no requirement of a very large weak value. That is, the final output intensity is still strong and measured data are stable. Our result suggests that this technique may become an alter-

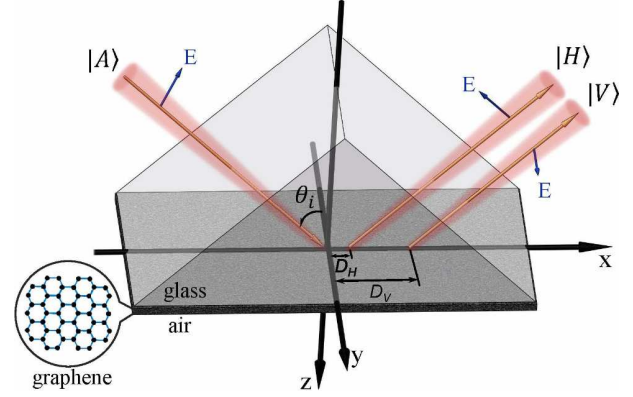


FIG. 1: (color online) Schematic illustrating the GH shift in graphene under TIR. A  $45^\circ$  linearly polarized beam labeled by  $|A\rangle$  hits a glass-graphene-air interface at an incident angle  $\theta_i$ . Then the components  $|H\rangle$  and  $|V\rangle$  experience lateral small GH shifts  $D_H$  and  $D_V$ , respectively.

native way to effectively and conveniently identify layers of few-layer graphene.

Consider a reflection system shown in Fig. 1. An incoming beam is at the  $45^\circ$  linearly polarization state  $|A\rangle$ . Under a TIR condition, the reflected light consists of two beams, one is the horizontal ( $H$ ) component  $|H\rangle$  displaced by  $D_H$  and the other is the vertical ( $V$ ) component  $|V\rangle$  displaced by  $D_V$ . We only concern about the difference between  $D_V$  and  $D_H$  because it is the measured variable in our weak measurements scheme. To calculate the GH shift ( $D_V - D_H$ ) for different graphene layers, the obtainment of the reflection coefficient in the graphene-dielectric interface is important. The reflection coefficient here is given by [20, 34]

$$r_A = \frac{R_A + R'_A \exp(2idk_{gz})}{1 + R_A R'_A \exp(2idk_{gz})}. \quad (1)$$

Here,  $R_A$  and  $R'_A$  are the Fresnel reflection coefficients in the glass-graphene and graphene-air interfaces, respectively,  $A \in \{H, V\}$ .  $k_{gz}$  is the component of wave vector  $k_0$  in graphene along  $z$  direction.  $d = \zeta \Delta d$  is the thickness of the graphene film with  $\zeta$  and  $\Delta d = 0.34\text{nm}$  representing the layer numbers and the thickness of single layer graphene, respectively. In TIR, the reflection coefficient  $r_A$  is complex and can be written as  $r_A = |r_A| \exp(i\varphi_A)$ . Neglecting the small angular shift due to the slow varia-

\*Electronic address: hailuluo@hnu.edu.cn

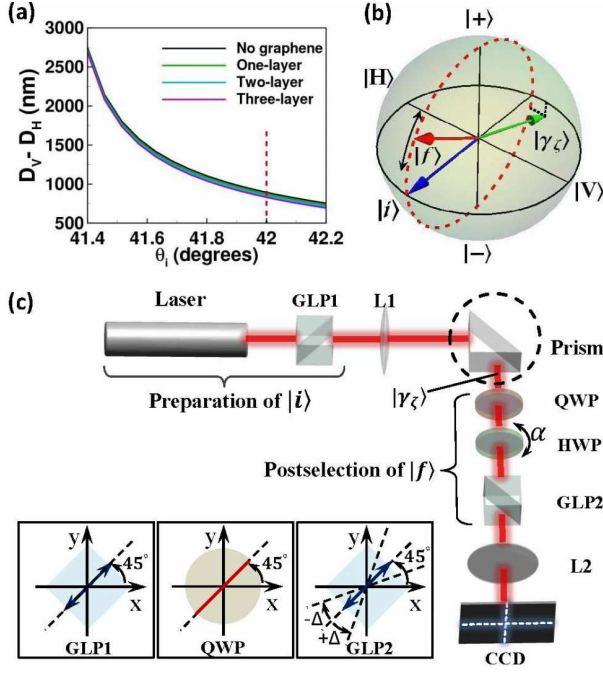


FIG. 2: (Color online) (a)  $(D_V - D_H)$  as a function of incident angle for different graphene layers. The red dashed line indicates the incident angle ( $42^\circ$ ) in our experiment, the angle of total reflection is  $41.3^\circ$ . (b) Representation on the Bloch sphere of the states  $|i\rangle$ ,  $|\gamma_\zeta\rangle$ , and  $|f\rangle$ .  $|i\rangle$  is the incident state and  $|f\rangle$  is the postselected state.  $|\gamma_\zeta\rangle$  is the preselected state after reflecting at the graphene-dielectric interface. The state  $|\gamma_\zeta\rangle$  is off to be antiparallel to  $|i\rangle$  in two angular directions depending on the graphene layer numbers. The red dashed circle represents the trajectory of  $|f\rangle$  when we rotate the half-wave plate (HWP). (c) Experimental setup: a Gaussian beam generated by a He-Ne laser (632.8nm, Thorlabs HNL210L-EC). GLP1 and GLP2, Glan Laser polarizers; QWP, quarter-wave plate; L1 and L2, lenses with focal length 125mm and 250mm respectively. The beam waist after L1 is  $71.25 \mu\text{m}$ . The data are detected by a CCD camera (Coherent LaserCam HR). Insets show the rotations of GLP1, QWP, and GLP2.

tion of  $|r_A|$  [15], the GH shifts for  $H$  and  $V$  components are spatial and can simply form as

$$D_A = -\frac{1}{nk_0} \frac{\partial \varphi_A}{\partial \theta_i}. \quad (2)$$

Here,  $n = 1.515$  is the refractive index of prism. From Eq. (2), we plot the curves of the GH shift as a function of incident angle for different graphene layers with the refractive indexes  $(3 + 1.149i)$  of graphene, as shown in Fig. 2(a). The shift decreases with increasing numbers of layer, but the decrement is tiny and all shifts are small.

To amplify these small shifts, the weak measurements are employed and the experimental setup is plotted in Fig. 2(c). This setup is similar to that prescribed in [29]. In a schema of weak measurements, the preselected state, postselected state, and weak coupling between the system and pointer are three key elements. The corresponding elements in our scheme will be clear in the following.

We first discuss the preselected state which is deli-

cate here due to the effect of reflection coefficients. In the experiment, we set the optical axis of GLP1 to  $45^\circ$  to project the incident polarization state on  $|i\rangle = (1/\sqrt{2}, 1/\sqrt{2})$ . And this polarization state changes to  $|\gamma_\zeta\rangle = F|i\rangle$  when the light is reflected at the interface.  $F$  is the reflection matrix [32]

$$F = \begin{bmatrix} -r_H & 0 \\ 0 & r_V \end{bmatrix}, \quad (3)$$

of which action is also a part of the preselection process, and the preselected state for our weak measurements scheme is  $|\gamma_\zeta\rangle$ . Note that the state  $|\gamma_\zeta\rangle$  is an elliptical polarization state which is different for one, two, and three graphene layers. Then we consider the weak coupling. The tiny GH effect is regarded as a weak measuring process here, as labeled by the dashed circle in Fig. 2(c). In the language of quantum mechanics, this effect described by operator is [6, 30, 31]

$$\hat{G}H = \begin{bmatrix} D_H & 0 \\ 0 & D_V \end{bmatrix}. \quad (4)$$

We next analyze the postselection, which can be realized by the combination of QWP, HWP, and GLP2. In the experiment, the optical axis of QWP is fixed to  $45^\circ$  from the  $x$  axis, and the rotation angle of HWP is  $\alpha$ . These settings described by the Jones matrices are

$$\begin{aligned} \text{QWP} &= \frac{1}{\sqrt{2}} \begin{bmatrix} 1 & -i \\ -i & 1 \end{bmatrix} \\ \text{HWP} &= \begin{bmatrix} \cos(2\alpha) & \sin(2\alpha) \\ \sin(2\alpha) & -\cos(2\alpha) \end{bmatrix}. \end{aligned} \quad (5)$$

The optical axis of GLP2 is  $(45^\circ \pm \Delta)$  to project on the state

$$\langle \text{GLP2} | = [\cos(45^\circ \pm \Delta) \quad \sin(45^\circ \pm \Delta)]. \quad (6)$$

Putting Eqs. (5) and (6) together, we obtain the postselected state as

$$\langle f | = [e^{i(2\alpha \mp \Delta)} \quad -e^{-i(2\alpha \mp \Delta)}]. \quad (7)$$

For convenience, we represent above states  $|i\rangle$ ,  $|\gamma_\zeta\rangle$ , and  $|f\rangle$  on the Bloch sphere, as shown in Fig. 2(b). One can see that the postselected state  $|f\rangle$  is limited on the red dashed circle by adjusting HWP [from Eq. (7)]. For the preselected state  $|\gamma_\zeta\rangle$ , it exhibits a deviation from the red dashed circle on the Bloch sphere in Fig. 2(b) [see Fig. 3(a) for the cases of different layers]. The reason for this deviation is that  $|r_H| \neq |r_V|$  and the difference between  $|r_H|$  and  $|r_V|$  increases with the increased layers of graphene.

With the preselected and postselected states discussed above, the weak value in our weak measurements can be obtained as

$$\frac{\langle f | \hat{G}H | \gamma_\zeta \rangle}{\langle f | \gamma_\zeta \rangle} = \frac{1}{2}(D_H + D_V) + \frac{A_w}{2}(D_H - D_V), \quad (8)$$

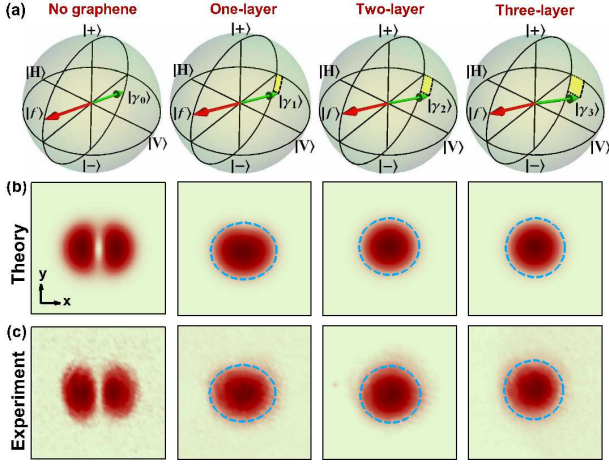


FIG. 3: (Color online) (a) Representation on the Bloch sphere of the state  $|\gamma_\zeta\rangle$  and  $|f\rangle$  when the tunable state  $|f\rangle$  is closest orthogonal to  $|\gamma_\zeta\rangle$  (reading intensity on CCD becomes minimum). The yellow area indicates the deviation to the circle of  $|f\rangle$ . (b) The theoretical minimum intensity by adjusting HWP. (c) The corresponding minimum intensity we read out from CCD. Note that the first, second, third, and fourth columns correspond to the cases of no, one-layer, two-layer, and three-layer graphene, respectively.

where  $A_w = \langle f | \hat{\sigma}_3 | \gamma_\zeta \rangle / \langle f | \gamma_\zeta \rangle$ , and  $\hat{\sigma}_3$  is the Pauli matrix. Obviously, the weak value from Eq. (8) is related to  $\zeta$ , i.e., the layer of graphene. Here,  $A_w$  in all cases is a complex number except the one of  $\zeta = 0$ , in which it is pure imaginary, for the full study in different theory about this case one can see [29]. Note that the GH shift in TIR is a spatial shift (the angular GH shift is too small even in graphene), and the imaginary part of  $A_w$  can naturally convert the relevant spatial shift ( $D_H - D_V$ ) into an angular one. Therefore, in order to obtain the centroid position  $\langle x \rangle$  of the beams, the propagation effect in all cases should be considered [4, 21]. Containing Eq. (8),  $\langle x \rangle$  is obtained as

$$\frac{1}{2}[(D_H + D_V) + \text{Re}(A_w)(D_H - D_V) + \frac{z}{z_r} \text{Im}(A_w)(D_H - D_V)], \quad (9)$$

where  $z_r$  is the Rayleigh range and  $z$  is the propagation. In fact, the shift we measure in the experiment is a relative position of the beams on CCD for the postselected states with  $\pm\Delta$ . Thus, the third term in Eq. (9) is pivotal and the first term is irrelative. The second term mainly results from the inequality between  $|r_H|$  and  $|r_V|$ .

We now turn to the procedure for experimentally observing amplified GH shift. The rotations of GLP1 and QWP are all fixed at  $45^\circ$ . We first set GLP2 to  $45^\circ$ , i.e.,  $\Delta = 0$ . Then we rotate the HWP with an angle  $\alpha$  and the state  $|f\rangle$  will project on the red dashed circle in Fig. 2(b). Note that the rotation  $\alpha$  is different for different layers of graphene, but it is unnecessary to clarify it in the experiment. We adjust the HWP until the output intensity on CCD becomes minimum, which indicates that the postselected state  $|f\rangle$  is closest orthogonal to the preselected

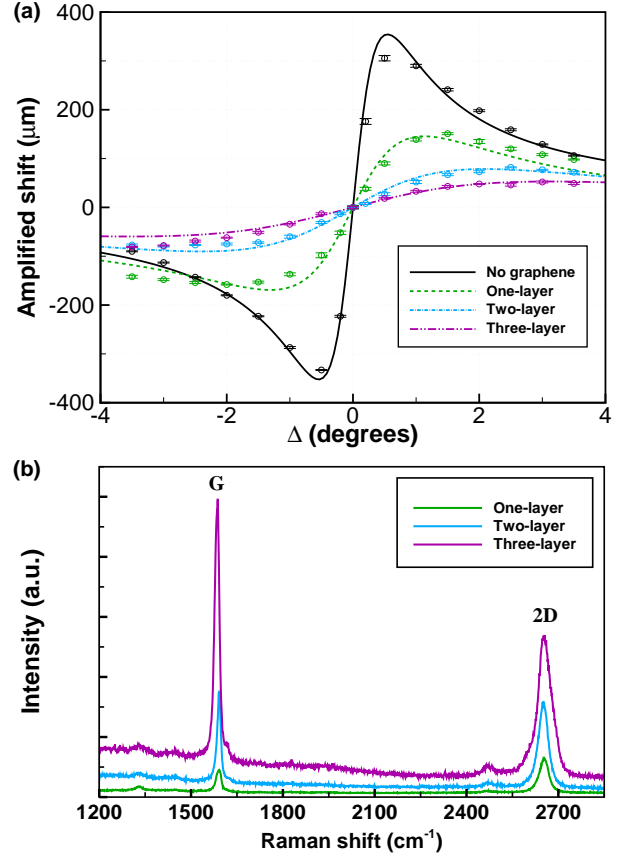


FIG. 4: (Color online) (a) The amplified shift as the function of angle  $\Delta$  for different graphene layers. Experimental data are shown as open dots with error bars. (b) Raman spectrum of our samples for one-layer, two-layer, and three-layer graphene.

state  $|\gamma_\zeta\rangle$ . After minimizing the output intensity, we rotate the GLP2 first to  $(45^\circ + \Delta)$  and then to  $(45^\circ - \Delta)$  to measure the final amplified shift.

As discussed above, we use a quantum mechanical description to analyze the amplified GH shift in order to provide a good physical insight and simplify the analysis. In fact, the process for the weak measurement of GH effect can be described by using standard wave optics [29], and the simulative minimum output intensity is illustrated in Fig. 3(b). We see that only in the case of no graphene the minimum intensity exhibits double-peak profile, which is a common distribution of minimum output intensity in weak measurements [26]. This is because in this case the state  $|f\rangle$  is possible to be orthogonal to  $|\gamma_0\rangle$ . For other cases with the existence of graphene, the tunable postselected state can not be orthogonal to the preselected state, and the nonorthogonal degree becomes larger when the layers of graphene increase, leading to a smaller weak value. As a result, the minimum intensity tends to a Gaussian form [33]. The corresponding minimum intensity we experimentally observe is shown as Fig. 3(c).

We measure the amplified GH shifts in no, one-layer,

two-layer, and three-layer graphene. The theoretical results of the amplified shift are briefly described by Eq. (9). However, in order to avoid the approximate limits and get accurate values, the curves in Fig. 4(a) are given by a precise weak measurement theory [27]. For a fixed angle  $\Delta$ , the amplified shift decreases with increasing layers. Thus, we can conveniently determine the layers of a sample at a special angle. In our experiment, each sample we fabricate is uniform layer and the size of sample is 1cm\*1cm. In practice, we repeat the experiment of weak measurements several times in different measuring place for each sample and the data are nearly same. To confirm the corresponding layers of graphene film, we provide their Raman spectra in Fig. 4(b). The layers of each sample deduced from our data coincide well with the results from Raman spectra.

The measurability of very small displacements is ultimately limited by the quantum noise of the light, because enough photons need to be collected to resolve the position of the field [21]. Note that another interesting beam shift induced by photonic spin Hall effect can also be used to identify graphene layers [34]. In that case, the experimental measurement was performed near Brewster angle. Therefore, the experimental data are a little unstable due to a low reflection intensity near Brewster angle. In present case, however, enough photons can be captured

by the detector due to the TIR. From the error bars in Fig. 4(a), we see that the data read from CCD are very stable. We recently noted that a similar experimental setup can also be used to observe the angular and lateral GH shifts near the critical angle for TIR [35].

In conclusion, we have experimentally observed the GH shift in graphene via weak measurements. Theoretically, the variations of the initial shifts for no, one-layer, two-layer, and three-layer graphene are tiny. However, employing a weak value amplification scheme, the amplified GH shift decreases with the increased layers of graphene. This technique may be utilized to identify layers of few-layer graphene with the stable data of this system. Our research is important for the research of graphene in future and may offer the opportunity to characterize the parameters of graphene with the help of weak measurements.

### Acknowledgments

This research was supported by the National Natural Science Foundation of China (Grants Nos. 11274106 and 11474089); Hunan Provincial Innovation Foundation for Postgraduate (CX2016B099).

- 
- [1] F. Goss and H. Hänchen, *Ann. Phys.* **436**, 333 (1947).
  - [2] C. Imbert, *Phys. Rev. D* **5**, 787 (1972).
  - [3] F. I. Fedorov, *Dokl. Akad. Nauk SSSR* **105**, 465 (1955).
  - [4] A. Aiello and J. P. Woerdman, *Opt. Lett.* **33**, 1437 (2008).
  - [5] M. R. Dennis and J. B. Götte, *New J. Phys.* **14**, 073013 (2012).
  - [6] F. Töppel, M. Ornigotti, and A. Aiello, *New J. Phys.* **15**, 113059(2013).
  - [7] K. Y. Bliokh and A. Aiello, *J. Opt.* **15**, 014001 (2013).
  - [8] M. Ornigotti, A. Aiello, and C. Conti, *Opt. Lett.* **40**, 558 (2015).
  - [9] H. M. Lai and S. W. Chen, *Opt. Lett.* **27**, 680 (2002).
  - [10] H. Gilles, S. Girard, and J. Hamel, *Opt. Lett.* **27**, 1421 (2002).
  - [11] D.-K. Qing and G. Chen, *Opt. Lett.* **29**, 872 (2004).
  - [12] X. Yin and L. Hesselink, *Appl. Phys. Lett.* **89**, 261108 (2006).
  - [13] J. He, J. Yi, and S. He, *Opt. Express* **14**, 3024 (2006).
  - [14] M. Merano, A. Aiello, G. W. 't Hooft, M. P. van Exter, E. R. Eliel, and J. P. Woerdman, *Opt. Express* **15**, 15928 (2007).
  - [15] S. Grosche, M. Ornigotti, and A. Szameit, *Opt. Express* **23**, 30195 (2015).
  - [16] N. Hermosa, *J. Opt.* **18**, 025612 (2016).
  - [17] J. C. Martinez and M. B. A. Jalil, *Europhys. Lett.* **96**, 27008 (2011).
  - [18] M. Cheng, P. Fu, X. Chen, X. Zeng, S. Feng, and R. Chen, *J. Opt. Soc. Am. B* **31**, 2325 (2014).
  - [19] W. J. M. Kort-Kamp, N. A. Sinitsyn, and D. A. R. Dalvit, *Phys. Rev. B* **93**, 081410(R) (2016).
  - [20] X. Li, P. Wang, F.i Xing, X.-D. Chen, Z.-B. Liu, and J.-G. Tian, *Opt. Lett.* **39**, 5574 (2014).
  - [21] O. Hosten and P. Kwiat, *Science* **319**, 787 (2008).
  - [22] P. B. Dixon, D. J. Starling, A. N. Jordan, and J. C. Howell, *Phys. Rev. Lett.* **102**, 173601 (2009).
  - [23] Y. Qin, Y. Li, H. He, and Q. Gong, *Opt. Lett.* **34**, 2551 (2009).
  - [24] X. Zhou, Z. Xiao, H. Luo, and S. Wen, *Phys. Rev. A* **85**, 043809 (2012).
  - [25] Y. Aharonov, D. Z. Albert, and L. Vaidman, *Phys. Rev. Lett.* **60**, 1351 (1988).
  - [26] I. M. Duck, P. M. Stevenson, and E. C. G. Sudarshan, *Phys. Rev. D* **40**, 2112 (1989).
  - [27] A. G. Kofman, S. Ashhab, and F. Nori, *Phys. Rep.* **520**, 43 (2012).
  - [28] J. Dressel, M. Malik, F. M. Miatto, A. N. Jordan, and R. W. Boyd, *Rev. Mod. Phys.* **86**, 307 (2014).
  - [29] G. Jayaswal, G. Mistura, and M. Merano, *Opt. Lett.* **38**, 1232 (2013).
  - [30] S. Goswami, S. Dhara, M. Pal, A. Nandi, P. K. Panigrahi, and N. Ghosh, *Opt. Express* **24**, 6041 (2016).
  - [31] G. Jayaswal, G. Mistura, and M. Merano, *Opt. Lett.* **39**, 6257 (2014).
  - [32] J. B. Götte and M. R. Dennis, *Opt. Lett.* **38**, 2295 (2014).
  - [33] S. Chen, X. Zhou, C. Mi, H. Luo, and S. Wen, *Phys. Rev. A* **91**, 062105 (2015).
  - [34] X. Zhou, X. Ling, H. Luo, and S. Wen, *Appl. Phys. Lett.* **101**, 251602 (2012).
  - [35] O. J. S. Santana, S. A. Carvalho, S. De Leo, and L. E. E. De Araujo, *Opt. Lett.* **41**, 3884 (2016).